

Solid Ink Laser Patterning for High-Resolution Information Labels with Supervised Learning Readout

Sebastian Ronneberger, Junfang Zhang, Yuxin Liu, and Felix F. Loeffler*

Tagging, tracking, or validation of products are often facilitated by inkjet-printed optical information labels. However, this requires thorough substrate pretreatment, ink optimization, and often lacks in printing precision/resolution. Herein, a printing method based on laser-driven deposition of solid polymer ink that allows for printing on various substrates without pretreatment is demonstrated. Since the deposition process has a precision of $<1\ \mu\text{m}$, it can introduce the concept of sub-positions with overlapping spots. This enables high-resolution fluorescent labels with comparable spot-to-spot distance of down to $15\ \mu\text{m}$ ($444,444\ \text{spots cm}^{-2}$) and rapid machine learning-supported readout based on low-resolution fluorescence imaging. Furthermore, the defined thickness of the printed polymer ink spots can be used to fabricate multi-channel information labels. Additional information can be stored in different fluorescence channels or in a hidden topography channel of the label that is independent of the fluorescence.

1. Introduction

Optical information labels are indispensable. They are not only used to convey product information, but also for security, tracking, and validation purposes.^[1,2] Among different optical information devices, fluorescent labeling is one of the most common and effective strategies. Complex information can be stored in multi-channel fluorescent labels.^[3] Although numerous methods for the generation of fluorescent labels are reported, based on for instance laser cutting,^[4] direct laser

writing,^[5,6] nanoprining,^[7,8] or lithography techniques,^[9,10] these often face limitations in material flexibility, expensive setup, and tedious processing steps. Recent methods involving perovskites now even allow for writing and erasing of information,^[6] but typically contain toxic lead compounds and face rapid degradation and a narrow substrate scope.^[8,10,11] Thus, inkjet printing is often the choice for information and security label generation, which is low-cost, fast, and relatively easy to implement with precise control over the pattern.^[1,2,12,13]

However, surface compatibility is a big challenge for inkjet printing. The substrates have to undergo pre-treatment steps,^[14] and individually optimized inks for specific functional materials are necessary to guarantee a high-quality pattern.^[15,16]

This requires considerable time for a fine tuning of ink parameters, such as solvents, additives, viscosity, homogeneity, and others.^[17,18] Furthermore, the precision of standard inkjet printers is limited to $\approx 5\text{--}10\ \mu\text{m}$,^[19,20] because the ejection and deposition of smaller solvent droplets become less precise. This is mainly due to variations in droplet formation and ejection at the nozzle tip, caused by inhomogeneous solvent surface tension, evaporation, and wetting behavior, aggravated by the long traveling distance between the nozzle and substrate.^[21,22] The droplet deposition precision can be improved using enhanced printing techniques, such as electrohydrodynamic inkjet printing, but demands a conductive support and high voltages, while being significantly slower.^[20,23] Moreover, drying of the pattern can cause varying results (e.g., Coffee ring effect, ink spreading)^[24,25] or the solvent may harm sensitive surfaces.


Therefore, new techniques are required that allow for printing with high precision and resolution, resulting in smaller security labels and/or higher information density, as well as enabling printing on various substrates without ink optimization or surface pretreatment. A solution to this can be the printing of solid inks, where the classical (liquid) solvent is replaced by an at room temperature solid polymer.

In this work, we developed a high-precision fluorescent label printing process, based on our approach of laser-induced forward transfer of polymers (polyLIFT). Conventional LIFT approaches typically rely on ultrashort (femto- to nanosecond) laser pulses for transferring thin-film surface patterns,^[26–28] used as chemical sensors,^[29] organic thin-film transistors,^[30] or organic photovoltaics.^[31] In comparison, our method uses a low-cost continuous wave laser, pulsed in

S. Ronneberger, J. Zhang, Y. Liu, F. F. Loeffler
Max-Planck-Institute of Colloids and Interfaces
Am Muehlenberg 1, 14476 Potsdam, Germany
E-mail: felix.loeffler@mpikg.mpg.de

S. Ronneberger
Institute of Physics and Astronomy
University of Potsdam
Campus Golm, Karl-Liebknecht-Straße 24/25, 14476 Potsdam, Germany

J. Zhang, Y. Liu
Institute of Chemistry and Biochemistry
Free University of Berlin
14195 Berlin, Germany

 The ORCID identification number(s) for the author(s) of this article can be found under <https://doi.org/10.1002/adfm.202210116>.

© 2023 The Authors. Advanced Functional Materials published by Wiley-VCH GmbH. This is an open access article under the terms of the Creative Commons Attribution License, which permits use, distribution and reproduction in any medium, provided the original work is properly cited.

DOI: 10.1002/adfm.202210116

Table 1. Comparison of inkjet printing and polyLIFT.

	Inkjet printing	polyLIFT
Deposition process	Jetting of liquid ink by thermal or mechanical shockwave generation	Melting of solid polymer matrix by laser
Ink storage	Reservoir, e.g., cartridge	Stock solution or spin-coated film on donor slide
Typically deposited droplet volume	μL – pL	fL
Typical printing precision	≈ 5 – $10\ \mu\text{m}$	$< 1\ \mu\text{m}$
Substrate pre-treatment	Ink/surface wetting optimization, surface plasma etching, or functionalization	Not required
Post-treatment	Drying of ink necessary	None (solid ink)

the micro to millisecond range, to print different molecules embedded in a polymer (solid ink). Recent advances in our technology, such as theoretical process understanding,^[32] compatibility with different polymers,^[33,34] robotic automation for high-throughput chemical synthesis,^[35] and a new nanolayer absorber for high resolution,^[34] have enabled various different applications in biotechnology, chemistry, and materials research. In the previous work, we used the polyLIFT process to generate patterns of covalently attached fluorescent positional isomers for message encryption, using acid vapor as the key for decryption.^[36] Building on these advancements and further optimizing the laser focus by size reduction of 31% in comparison to our previous work,^[37] we now show that polyLIFT technique enables a material printing precision of $< 1\ \mu\text{m}$ (see Figures S1–S3, Supporting Information), which is much higher than standard inkjet printers (see Table 1 for comparison of polyLIFT and inkjet). Without adjusting the polymer matrix or printing process, our technique enables printing on multiple substrates, such as paper, glass, aluminum, or plastic foil. Since the printing process is solvent-free, it is much less prone to contamination or misprinting by nozzle clogging.

By exploiting these new high-resolution printing capabilities together with the solid ink property of polyLIFT, we could introduce a sub-position writing approach. Each position is composed of multiple overlapping sub-spots, which can now be deconvoluted by a machine learning algorithm to read the data. This allowed us to create patterns with much higher data density than recently reported inkjet-printed binary information

storage,^[3] with only two (instead of seven) fluorophores and a simple fluorescence scanner (without high-resolution confocal microscopy). Finally, an encryption by two independent read-out channels was established, where in addition to the fluorescence signal, also the spot topography (height information) in the nanometer regime can be used for data encoding. The topography information layer can not only store additional information, but may also act as a hidden channel to increase the security of a label.

2. Results and Discussion

The LIFT-based fluorescence labeling process begins with a donor slide that is covered with a laser absorber layer and a spin-coated polymer (i.e., the solid ink), containing fluorescent molecules (Figure 1). The donor is placed in direct contact with an acceptor slide, reducing the transfer distance to a minimum. Then, the laser absorber is locally heated by a laser in a defined pattern, the polymer is transferred from the donor onto the acceptor slide, and solidifies directly after transfer. On a technical side, this solvent-free printing technique is enabled by a laser setup equipped with a 488 nm diode laser, which is tightly focused by an optical system onto the nano-absorber layer of the donor slide. Using a scan head with mirrors mounted on galvanometer scanners and an f-theta lens, the focused laser spot can be positioned in $< 1\ \mu\text{m}$ precision (Figures S1–S3, Supporting Information), with scanning velocities of up to several hundred mm s^{-1} .

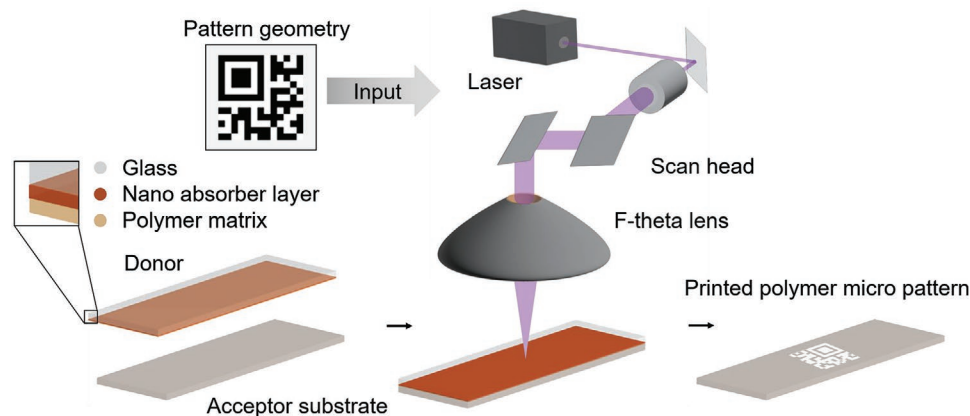


Figure 1. Overview of polymer micropattern printing process with the polyLIFT method. A focused laser beam transfers the polymer matrix from the donor onto the acceptor substrate, defined by the irradiation pattern.

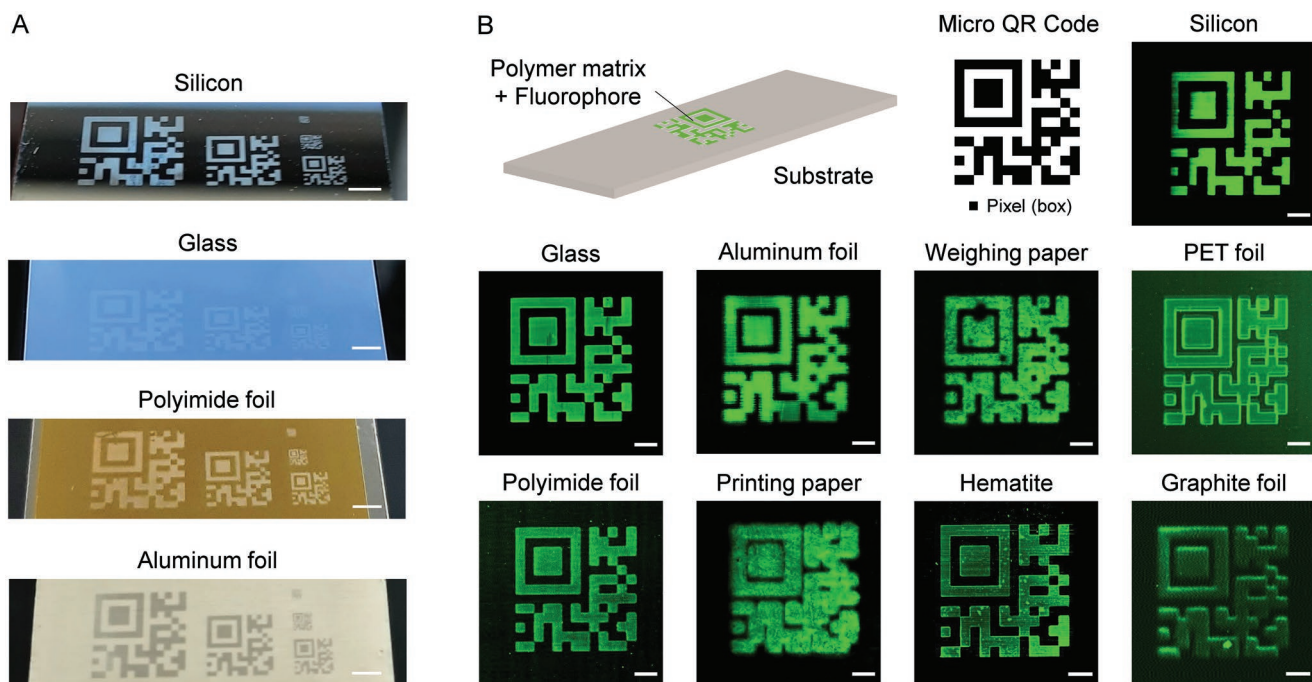


Figure 2. A) Printing on investigated substrate collection. Scale bar 2 mm. B) Fluorescence scans of printed fluorophore doped polymer micro QR codes on different substrates. Scale bars 500 μm .

Using this setup, we investigated the printing of solid ink fluorescence labels on various commercially available substrates: silicon, glass, aluminum foil, weighing and printing paper, hematite, polyethylene terephthalate (PET), polyimide, and graphite foil. The different substrates were chosen due to their ubiquitous use in packaging for pharmaceutical products, food, and electronics/semiconductors, as well as surface finishes for displays, watches, or documents. Commonly, inkjet printing is used for label generation on these substrates, but the ink has to be optimized for each substrate surface individually and pre-treatment steps are necessary. With our setup, we printed the same solid ink consisting of polystyrene (PS), mixed with the fluorescent dye Rhodamine 6G, in form of micro QR codes onto each substrate. Furthermore, the same transfer parameters (89 mW laser power, 4000 dpi resolution, laser on time 400 μs per dot) were used for all substrates and no pre-treatments of the acceptor surfaces were performed. We selected commercially available PS due to its favorable properties, such as outstanding LIFT processability (largest material amounts transferred in our approach),^[33] suitable hydrophobicity, glass transition temperature, low-cost, and widespread use.

The example micro QR code with the encoded data “MPI KG” had a pattern geometry of 13×13 pixels with single QR code pixel (box) sizes of 500, 350, 200, 100, and 50 μm (Figure 2A) corresponding to QR code dimensions from 6.5 mm \times 6.5 mm to 0.65 mm \times 0.65 mm. For silicon, glass, polyimide, and aluminum foil, which have a microscopically flat surface, the printed micro QR codes are visible to eye.

All investigated substrates were scanned by a fluorescence scanner in the 532 nm channel at a resolution of 5 μm pixel⁻¹ to determine the maximum printing resolution

(see Experimental Section part for substrate handling). The fluorescence scans of the micro QR codes on various substrates (Figure 2B) reveal that the highest possible resolution is 200 μm pixel⁻¹ (= QR code individual box size) for printing paper. However, much higher resolutions can be achieved on very flat surfaces, such as glass and silicon, by decreasing the box size or adapting the printing mode (see Figure 3). The micro QR codes can be printed by using an area transfer approach, where the area is printed by numerous overlapping spot transfers, which form a homogeneous polymer layer (see Figure S4, Supporting Information). To increase the pattern resolution, each box of the micro QR code can be represented by a single polymer microspot. As we have recently reported,^[34] the hematite nanoabsorber enables a minimum spot-to-spot distance (pitch) of 30 μm and thus marks the current resolution limit for this transfer mode.

However, exploiting the solid ink property together with the micrometer exact positioning of the laser spot, an even higher printing resolution can be achieved by introducing a sub-position concept (Figure 3C,D). Each spot/position consists of four sub-position, arranged in a 2×2 grid, with the center point being the original spot coordinate. Each sub-position is shifted from this coordinate by 4–10 μm offset in x and y directions. To apply the sub-position concept on a micro QR code and enable machine learning-based readout, the pattern is rasterized into 2×2 segments containing two micro QR code boxes in each dimension. The offset can be tuned to result in a well-defined overlap of the polymer spots, generating characteristic 2×2 overlapping spot patterns in each position, with a minimum pitch of down to 30 μm . Therefore, by using this sub-position concept, it is possible to increase the resolution by a factor of four, enabling a pitch of 15 μm . This concept is not possible to

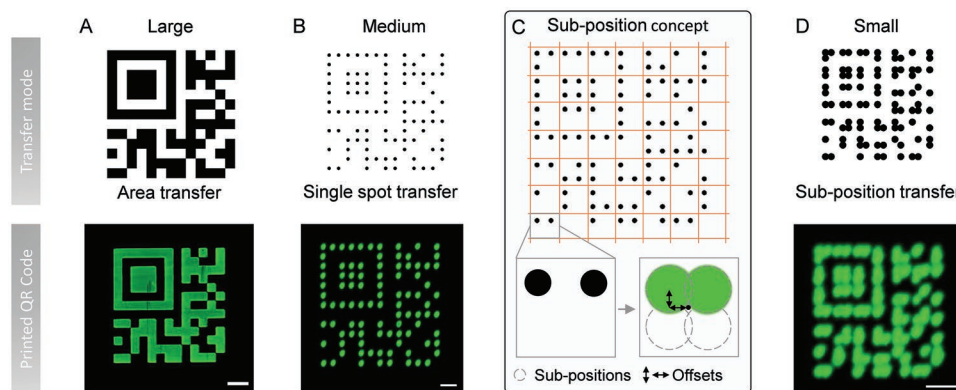


Figure 3. Different printing modes of the same QR code, reaching different pattern sizes on standard microscope glass. A) Large-scale printing by area transfer mode (scale bar 500 μm). B) Medium size printing with single polymer spot transfers (scale bar 100 μm). C, D) By introducing the sub-position concept, an even higher resolution can be achieved (scale bar 50 μm).

use with inkjet printing, since the printing precision is too low and the liquid ink spots tend to merge, dry, and/or dewet.

The sub-positions can be automatically read out (Figure 4A), due to the characteristic 2×2 segments, which is ideal for a machine learning-based recognition. In contrast, a continuously overlapping spot pattern would be much more challenging to segment, analyze, or train an algorithm, due to cross talk from neighboring overlapping spots, as we show later (Figure 4B). Therefore, first, the fluorescence image is

segmented into individual tiles containing a sub-position at one grid coordinate. Next, the stack of sub-position tiles is analyzed by a pre-trained support-vector machine (SVM).

The SVM was trained with artificial data of random sub-position states (see Experimental Section part) and, afterward, the prediction was validated. This approach allows a fast and automatic data readout.

Since the pattern recognition is influenced by the sub-position pattern geometry (sub-position offset and position

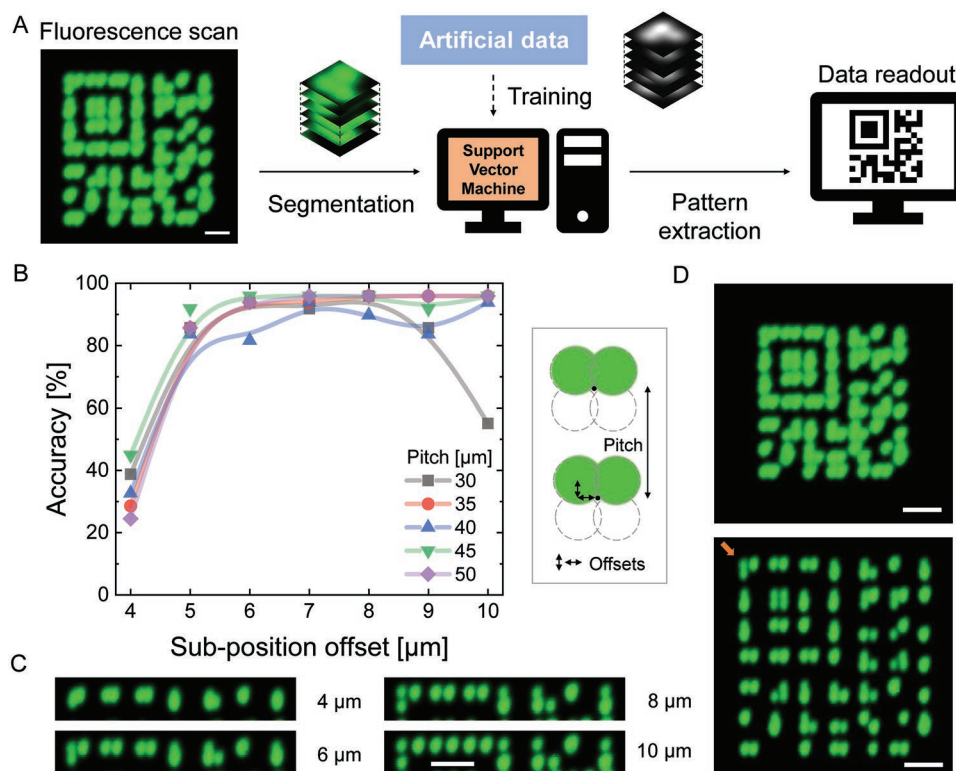


Figure 4. Micro QR codes printed with sub-position concept on standard microscope glass. A) Automated data read-out of sub-position pattern using a support-vector machine algorithm. B) Accuracy study with different sub-position offsets and pitches. C) Examples of different sub-position offsets with 40 μm pitch. D) QR codes with sub-position concept printed with offset of 6 μm and a pitch of 30 μm (top) and 40 μm (bottom). Scale bars A: 30 μm , C and D: 50 μm .

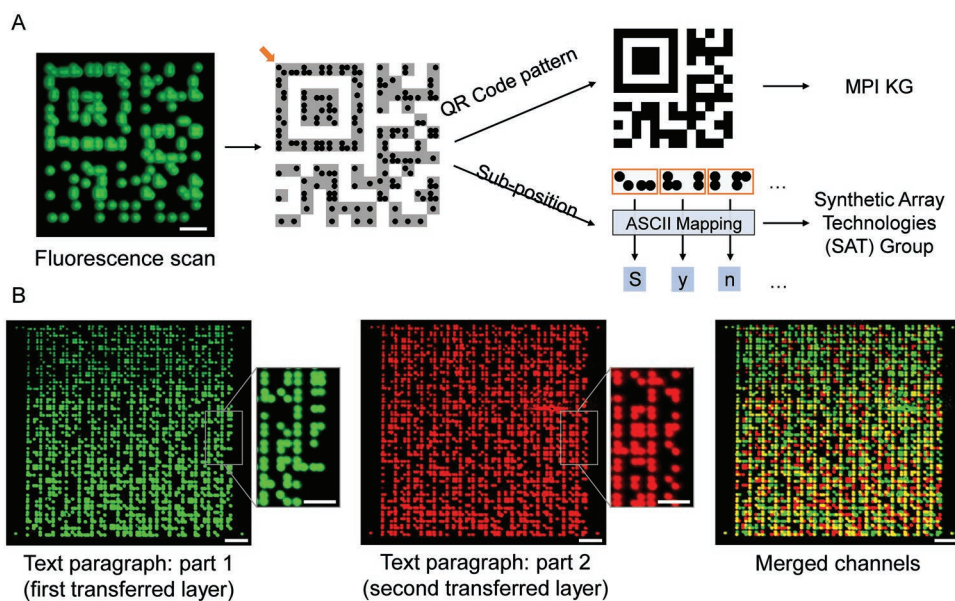


Figure 5. A) Two-level information label on glass. The macroscopic arrangement generates a QR code pattern and individual sub-positions encode an additional information layer. Orange arrow marks the starting point of the ASCII string. Fabricated with a pitch of 45, 8 μm offset, 50.5 mW laser power, 400 μs irradiation time, and 5 ms delay time. Scale bar: 100 μm . B) Two fluorophore pattern on glass, storing an ASCII text encoded with sub-positions in two independent fluorescence channels. The pattern was printed with a pitch of 55 μm , 9 μm sub-position offset, laser power of 82.6 mW, delay time of 5 ms, and 400 μs irradiation time. Scale bars: 100 μm .

pitch), a parameter study was carried out to investigate optimal printing parameters. Therefore, offset values from 4–10 μm with 1 μm interval as well as pitch values of 30–50 μm in 5 μm intervals were screened (see Figures S5–S9, Supporting Information). For all micro QR code patterns, a laser power of 50.5 mW, 400 μs irradiation time, and 5 ms delay time between consecutive spot transfers were used. Analyzing different micro QR code geometries (Figure 4B), the SVM shows a low accuracy for small sub-position offsets of 4 and 5 μm . This results from a strong overlap of the sub-positions, making pattern detection very difficult. Sub-position patterns that were printed with an offset of 6 μm and larger generally show a high accuracy of > 90%. However, for 10 μm offset and 30 μm pitch, cross talk (overlapping signals) from neighboring positions decreases the accuracy again. The best accuracy and resolution can be obtained with 6 μm sub-position offset, which can also be observed by visual inspection (Figure 4C). Two representative micro QR code patterns with 6 μm sub-position offset and pitches of 30 and 40 μm (Figure 4D) resulted in read-out accuracies of 93.9% and 81.6%. The reduced accuracy for the 40 μm pattern could emerge from slight local inhomogeneities in the nano-absorber layer, which can influence the polymer transfer.

The sub-position concept can be also applied to two-level information labels (Figure 5A). Therefore, each 2×2 sub-position tile is arranged into a large-scale micro QR code pattern, forming the first information layer. This can be read out by calculating the total fluorescence intensity for each tile, independent of the sub-positions, and comparing against a threshold value, encoding for 0 and 1. However, to achieve a “1” in this information layer, despite the case that sometimes all 2×2 sub-positions need to be empty, we had to apply a change: to encode a “1”, the empty 2×2 sub-position was replaced by

printing a single polymer microspot at the center coordinate (= tile center).

The second level of information is stored in the individual sub-positions and is numerated and assigned reading row-wise from left to right. Two adjacent positions (eight sub-positions) enable 256 combinations to form a byte, which is used to store one ASCII character.

We generated a two-level information label, where the first level of the micro QR code stores the information “MPI KG” and the sub-positions encode the string “Synthetic Array Technologies (SAT) group”.

While the first information level “MPI KG” is simple to read by analyzing the tiles with a threshold, the second information level with sub-positions has to be extracted and analyzed by the SVM to obtain the text message “Synthetic Array Technologies (SAT) group”. Using the pretrained SVM an accuracy of 83.8% was obtained (see Figure S10, Supporting Information). This lower value in comparison to the previous parameter study results from introducing the grid center spot for a “1” in the first information level (= empty sub-positions), which is difficult to distinguish from other sub-position labels. These two-level information labels can be used for applications, where the amount of read out information should be limited by the fluorescence scan resolution. For instance, a low-resolution fluorescence scan can detect the information of the QR code, but for revealing the second information layer with the ASCII text message, a high-resolution scan in combination with SVM analysis of the sub-positions is needed.

Another possibility to increase the information density of the labels is to use multiple fluorophores (Figure 5B). We encoded the 27th paragraph of G.G. Stokes’ publication “On the Change of Refrangibility of Light”,^[38] where “fluorescence”

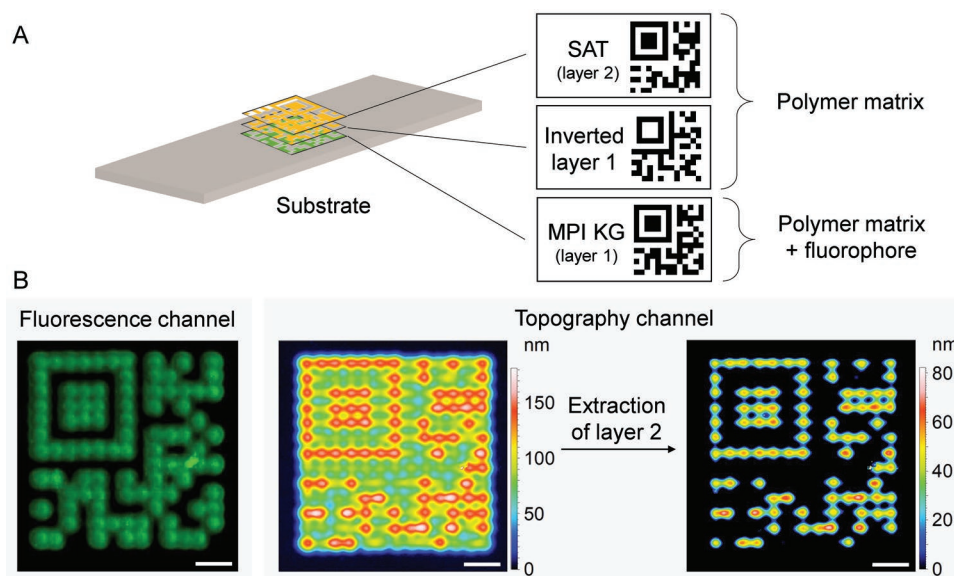


Figure 6. A) Dual channel information storage on glass. A fluorescence and topography layer can be used for orthogonal encoding of information into the polymer microspots. B) Left: Fluorescence channel (532 nm excitation). Right: Topography channel with height information of complete polymer pattern and after extraction of the second information layer via threshold method (set to 99 nm above the lowest point on the surface). Transfer parameters were 40 μm pitch, 10 μm sub-position offset, 63.9 mW laser power, 400 μs irradiation time, and 5 ms delay time. Scale bars: 50 μm .

was introduced for the first time as an ASCII text (1023 bytes, see Figure S11, Supporting Information). The ASCII information was converted into sub-position tiles and separated into two parts. Then, we transferred the first part as a polymer spot pattern, containing the fluorescent dye Rhodamine 6G (green). Afterward, on top of this first pattern, we transferred the second part as another polymer pattern, containing the fluorescent dye Nile blue A (red). We generally did not observe any interference between two printed patterns in stacked layers. The automatic data readout using a pretrained SVM resulted in an accuracy of 91.8% for the 532 nm channel and 92.5% for the 635 nm channel (see Figure S12, Supporting Information). These high percentages show that the pretrained SVM can even handle intensity variations among different polymer spots in a pattern, without the need to define a specific intensity threshold. The printed label has an information density of 165.25 bytes mm^{-2} per fluorophore, resulting in 330.5 bytes mm^{-2} for the two fluorescence channels. In comparison to the recently reported concept based on inkjet printing of fluorophores,^[3] using seven different fluorophores and reaching an information density of up to 271.5 bytes mm^{-2} , our sub-position approach enables higher densities with only two fluorophores and without the need for an expensive confocal laser scanning microscope. By further increasing the number of dyes, we could reach much higher information densities.

Since our printing method uses solid ink, which is not affected by ink spreading, the generated information labels are not limited to encoding data into fluorescent dyes only. It is also possible to store data as height information in a second orthogonal channel, allowing to use different analysis techniques for channel specific data readout (Figure 6).

We can encode two different information in the form of micro QR codes, using fluorescence and topography of the polymer microspots. First, a micro QR code, containing the information “MPI KG”, was printed as layer one using

the polymer matrix doped with Rhodamine 6G (for calculation of total fluorescence intensity and threshold method, see Figure S13, Supporting Information). Afterward, the inverse pattern of the first layer was printed with polymer matrix without any fluorophores, using the same transfer parameters. This printing step fills the remaining unoccupied positions from the first layer with non-fluorescent polymer and generates a leveled surface for the second layer, which will store the topography-encoded data. As the second layer, a micro QR code with the data “SAT” was printed, using the same transfer parameters and polymer without fluorophores (for extraction of height and applying a threshold analysis, see Figure S14, Supporting Information). A fluorescence scanner and a vertical scanning interferometer (VSI) allow for rapid image acquisition with orthogonal information channels. For the data acquisition, a simple threshold approach suffices, since the pattern was printed using stronger laser parameters and without sub-position offset. This results in larger polymer spots, which are necessary for a good VSI measurement (see Figure S15, Supporting Information). To investigate a more realistic application of our technology, we performed different stability studies over longer times. We stored microQR patterns for 7 days under daylight, in darkness, or at 50 $^{\circ}\text{C}$, as well as performed multiple temperature cycles from -20 – 50 $^{\circ}\text{C}$ (see Figures S19–S24, Supporting Information). Fluorescence data show an expected decrease in intensity, which may be circumvented by using other fluorescent materials. Nevertheless, high accuracies were obtained, since the process relies on SVM data readout without the need for a threshold. Interestingly, thicker polymer patterns were much more stable (see Figures S19 and S20, Supporting Information) with only minor dewetting. Long-term stability of the samples from Figure 2 on different substrates shows good stability, even after 37 weeks of storage (see Figures S23 and S24, Supporting Information).

3. Conclusion

In this work, we investigated solid ink printing method by using the polyLIFT technology for information label generation on various substrates. In comparison to inkjet printing, the method does not require a substrate-specific ink optimization or substrate pretreatment, making it a rapidly implementable approach. It enables fluorescent labels with scalable information density from mm² sized patterns down to high-resolution patterns of < 200 × 200 μm² using the concept of sub-positions. Due to its high printing precision of < 1 μm, an ASCII text encoded into sub-position tiles with 30 μm pitch could reach an information density of 555.4 bytes mm⁻², while with two fluorophores a potential density of > 1110 bytes mm⁻² may be reached. Encoding with more fluorophores as well as using orthogonal information channels, such as height and fluorescence, this approach enables highly compact and complex (or hidden) information label fabrication, functioning as “WORM” (write-once-read-many) devices.

To further increase the information density of these labels in the future, two paths could be followed: 1) Decreasing the distance between the tiles of the sub-position approach. In our case, a simple threshold approach was less reliable than the SVM approach. Thus, an additional training of the SVM would be required with more complex training data, to cope with interfering fluorescence signals from neighboring spots/tiles (see Figure 4B, drop in 30 μm pitch with 10 μm offset). 2) Increasing the resolution of the printing approach. The current limitation of the polyLIFT printing resolution lies in the absorber layer of the donor slide. Since the production of this layer is currently based on simple spin coating (without clean room facilities) and annealing in an air oven, we face some inhomogeneity issues. For multilayer sub-position label applications with several fluorophores or an additional topography information layer, this restricts the printing to 40 or 50 μm tile pitch. This process highly depends on precise laser absorption and heat diffusion. While the laser focus position is highly precise (< 1 μm), the nano-absorption layer needs to be precisely produced, since small deviations in absorption cause spot diameter variations, reducing the maximum resolution. Future studies will also address the minimization of the delay time between the transfers of two spots, as well as further explore additional polymers for high-resolution labels. We have previously shown that for example also polylactic acid, various copolymers, polyvinyl chloride,^[33] or poly(dimethylacrylamide),^[39] can be compatible with our process. A low-cost version of the laser setup can enable this process in any lab.^[40] Concluding, the facile polyLIFT process enables quick labeling of a product with fluorescent information patterns.

4. Experimental Section

Laser Setup: The polyLIFT setup consisted of a 488 nm TOPTICA iBeam smart 488-S laser with a maximum output power of 111 mW (TOPTICA Photonics AG, Germany) and flexible tuning of laser power and pulse duration. A laser scanning system (Racoon 11, ARGES GmbH, Germany), equipped with an f-Theta lens (S4LFT5110/322, Sill Optics GmbH, Germany) directs the laser beam, achieving after fine adjustments a laser spot size of 1 e⁻² = 14.7–15.2 μm, which was 15.5–18.6% smaller as reported previously^[37] (see Figures S1 and S2,

Supporting Information). The laser patterns were generated using ScanMaster Designer software (version 3.2.21, Novanta Company). The sub-position coordinates were calculated by a python3 algorithm.

Donor Slide Fabrication: Glass donor slides with a hematite nano-absorber layer were fabricated using standard microscope glass slides (76 × 26 × 1 mm microscope slides, REF 1010412, Marienfeld, Germany) according to a previously published protocol.^[34] The slides were spin-coated using 450 μL solution at 70 rounds per second. For the spin-coating solution, polystyrene with an average molar weight of 35000 (Sigma–Aldrich, CAS: 9003-53-6) was dissolved in toluene to obtain a concentration of 50 mg mL⁻¹. Rhodamine 6G (Acros organics, CAS: 989-38-8) and Nile blue A (Sigma–Aldrich, CAS: 3625-57-8) fluorescent dye stock solutions were prepared by pre-dissolving the fluorophores in DCM or DMF, respectively, with a concentration of 0.4 mg mL⁻¹. Rhodamine 6G (20 μL) stock solution and 80 μL of Nile blue A stock solution were added to 1 mL of the spin-coating solution directly before spin-coating.

Acceptor Substrate: For the acceptor substrate collection the following materials were tested: Aluminum foil (Universal aluminum foil, item No. 60010, Korff AG), PET foil (Melinex L4103, Plano GmbH, Germany), printing paper (multi-function paper 80 g m⁻², inapa tecno star), weighing paper (LOT 150211, Macherey-Nagel GmbH, Germany), polyimide foil (Kapton HN, DuPont, 25 μm polyimide layer with a 45 μm siloxane-based adhesive layer; CMC Klebtechnik), hematite slide (see),^[34] graphite foil (thermal conductive graphite foil – heat spreader, 17 μm thickness, Product No.: PG1512, ProGraphite GmbH), silicon substrate (with ≈ 5 nm thin silicon oxide layer, Siegert Wafer, Germany), and microscope glass slides (76 mm x 26 mm x 1 mm microscope slides, REF 1010412, Marienfeld, Germany).

The acceptor substrates were cut to a size of 26 mm x 76 mm and fixed on standard microscope glass slides for better handling, planarity, and fluorescence scanning.

All acceptor substrates were directly used without further pre-treatment. To remove dust grains, the surfaces were flushed with a jet of nitrogen shortly before printing. In case of silicon and glass as acceptor surfaces, a washing process was applied with acetone, isopropanol, and double-distilled water each for 5 min in an ultrasonic bath and dried in a jet of impurities.

Topography Measurement: A vertical scanning interferometer (smartWLI compact, Gesellschaft für Bild- und Signalverarbeitung (GBS) mgH, Illmenau, Germany) was used with 5× and 50× objectives for topographic measurements. Data analysis, such as leveling, form subtraction (3rd polynomial order), outlier removal, and stitching of measurement fields, were carried out in MountainsMap Version 8.0 (Digital Surf, France). The thickness of the hematite nano-absorber layer was measured with atomic force microscopy (see Figure S16, Supporting Information) and spin-coated polymer layer with smartWLI (see Figure S17, Supporting Information).

Fluorescence Imaging: Fluorescence images were obtained from a fluorescence scanner (Innopsys, Innoscan 1100 AL) at a pixel resolution of 1 μm and a scanning speed of 35. The 635 and 532 nm channels were simultaneously scanned using emission filters of 680/42 and 582/75 nm with detection gains of 5 and 0.2. The fluorescent labels on different acceptor substrates in Figure 2 were scanned with a Genepix scanner at a pixel resolution of 5 μm.

Fluorescent Pattern Decoding: Decoding of the fluorescent patterns was carried out automatically by using a trained support-vector machine (SVM). The SVM was implemented in python 3 using the scikit-learn package version 1.0.2.^[41] Training was carried out with artificially generated fluorescence image data assuming a spatial 2D Gaussian distribution in the fluorescence intensity (x,y):

$$I(x,y) = \sum_{n=1}^4 A_n e^{-\left(\frac{(x-x_{0,n})^2}{2\omega_x^2} + \frac{(y-y_{0,n})^2}{2\omega_y^2}\right)} + \text{Noise}_{(x,y)} \quad (1)$$

with intensity amplitude A , sub-position center coordinates x_0 , y_0 , standard deviation ω_x , ω_y , and constant Noise

accounting for background noise. The parameters A , x_0 , y_0 , ω_x , ω_y , and Noise were equipped with additional random variations, simulating variations/errors in the printing and fluorescence scanning processes. For the training of the SVM, a data set of 20000 artificially generated images was used with pitch and offset values corresponding to the specific transfer parameters. The values for ω_x and ω_y were estimated based on Gaussian fits on cross-section profiles of reference spot measurements (see Figure S18, Supporting Information). For the sub-position offset and pitch parameter study, ω_x and ω_y were set to 7 ± 1 and 9 ± 1 μm , respectively, whereas for the two-level information labels, ω_x and ω_y were set to 8.5 ± 1 and 7.7 ± 1 μm for Rhodamine 6G spots and 9.5 ± 1 and 7.5 ± 1 μm for Nile blue A spots.

Optimization of the model parameters C , γ , and the kernel was carried out with GridSearchCV using $C = [0.0001, 0.001, 0.01, 0.1, 1, 10, 100, 1000, \text{and } 10000]$, $\gamma = [0.0001, 0.001, 0.1, 1, 10, 100, 1000, \text{and } 10000]$, and kernel = ["rbf", "poly", and "linear"], resulting in $C = 0.0001$, $\gamma = 1$, and kernel = "poly" as best parameters.

A tile size of (39, 39) was used corresponding to $39 \mu\text{m} \times 39 \mu\text{m}$ for fluorescence scans at $1 \mu\text{m pixel}^{-1}$ resolution. The tile size was adapted for smaller pitches to reduce interactions from neighboring grid positions, resulting in sizes of (35, 35) and (30, 30) for 35 and 30 μm pitches. Training and test data were scaled to a range of [0,1] before feeding into the SVM.

For the dual channel information storage, a threshold method was used for extraction of the distinct micro QR codes (see Figures S13 and S14, Supporting Information).

Supporting Information

Supporting Information is available from the Wiley Online Library or from the author.

Acknowledgements

The authors would like to acknowledge the German Federal Ministry of Education and Research (BMBF, grant number 13XP5050A), the MPG-FhG Cooperation (Glyco3Display), the Max Planck Society, and the China Scholarship Council for financial support. The authors thank Reinhold Dünnebacke for the AFM measurements, Gerardo Hernández-Sosa, Dario Mager, and all members of the Synthetic Array Technologies group for fruitful discussions.

Open access funding enabled and organized by Projekt DEAL.

Conflict of Interest

The authors declare no conflict of interest.

Data Availability Statement

The data that support the findings of this study are available in the supplementary material of this article.

Keywords

inkjet printing, laser-induced forward transfer, machine learning, solvent-free polymer patterning

Received: August 31, 2022
Revised: January 10, 2023
Published online: February 3, 2023

- [1] Y. Liu, F. Han, F. Li, Y. Zhao, M. Chen, Z. Xu, X. Zheng, H. Hu, J. Yao, T. Guo, W. Lin, Y. Zheng, B. You, P. Liu, Y. Li, L. Qian, *Nat. Commun.* **2019**, *10*, 2409.
- [2] X. Zheng, Y. Zhu, Y. Liu, L. Zhou, Z. Xu, C. Feng, C. Zheng, Y. Zheng, J. Bai, K. Yang, D. Zhu, J. Yao, H. Hu, Y. Zheng, T. Guo, F. Li, *ACS Appl. Mater. Interfaces* **2021**, *13*, 15701.
- [3] A. A. Nagarkar, S. E. Root, M. J. Fink, A. S. Ten, B. J. Cafferty, D. S. Richardson, M. Mrksich, G. M. Whitesides, *ACS Cent. Sci.* **2021**, *7*, 1728.
- [4] J. Fei, R. Liu, *Mater. Sci. Eng., C* **2016**, *63*, 657.
- [5] A. O. Larin, L. N. Dvoretckaja, A. M. Mozharov, I. S. Mukhin, A. B. Cherepakhin, I. I. Shishkin, E. I. Ageev, D. A. Zuev, *Adv. Mater.* **2021**, *33*, 2005886.
- [6] X. Huang, Q. Guo, D. Yang, X. Xiao, X. Liu, Z. Xia, F. Fan, J. Qiu, G. Dong, *Nat. Photonics* **2019**, *14*, 82.
- [7] X. Lai, Q. Ren, F. Vogelbacher, W. E. I. Sha, X. Hou, X. Yao, Y. Song, M. Li, *Adv. Mater.* **2022**, *34*, 2107243.
- [8] J. S. Du, D. Shin, T. K. Stanev, C. Musumeci, Z. Xie, Z. Huang, M. Lai, L. Sun, W. Zhou, N. P. Stern, V. P. Dravid, C. A. Mirkin, *Sci. Adv.* **2020**, *6*, eabc4959.
- [9] Y. Zheng, C. Jiang, S. H. Ng, Y. Lu, F. Han, U. Bach, J. J. Gooding, *Adv. Mater.* **2016**, *28*, 2330.
- [10] P. Zhang, G. Yang, F. Li, J. Shi, H. Zhong, *Nat. Commun.* **2022**, *13*, 6713.
- [11] C. K. Lin, Q. Zhao, Y. Zhang, S. Cestellos-Blanco, Q. Kong, M. Lai, J. Kang, P. Yang, *ACS Nano* **2020**, *14*, 3500.
- [12] Y. Li, Z. Liu, K. Zhu, L. Ai, P. Jia, N. Wu, H. Yu, J. Wang, X. Yao, J. Zhou, Y. Song, *Adv. Mater. Interfaces* **2021**, *8*, 2101281.
- [13] L. Ding, X. D. Wang, *J. Am. Chem. Soc.* **2020**, *142*, 13558.
- [14] W. Lin, S. Gandhi, A. R. Oviedo Lara, A. K. Thomas, R. Helbig, Y. Zhang, *Adv. Mater.* **2021**, *33*, 2102349.
- [15] L. Zhou, L. Yang, M. Yu, Y. Jiang, C. F. Liu, W. Y. Lai, W. Huang, *ACS Appl. Mater. Interfaces* **2017**, *9*, 40533.
- [16] S. Schliske, C. Rosenauer, T. Rödlmeier, K. Giringer, J. J. Michels, K. Kremer, U. Lemmer, S. Morsbach, K. C. Daoulas, G. Hernandez-Sosa, *Adv. Mater. Technol.* **2021**, *6*, 2000335.
- [17] L. Wu, Z. Dong, F. Li, H. Zhou, Y. Song, *Adv. Opt. Mater.* **2016**, *4*, 1915.
- [18] N. F. Morrison, O. G. Harlen, *Rheol. Acta* **2010**, *49*, 619.
- [19] Scienion GmbH, sciFLEXARRAYER S12, <https://www.scienion.com/products/sciflexarrayer/sciflexarrayer-s12/#1600952449862-fe2d2c78-636e>, accessed: 08, **2022**.
- [20] J. U. Park, M. Hardy, S. J. Kang, K. Barton, K. Adair, D. K. Mukhopadhyay, C. Y. Lee, M. S. Strano, A. G. Alleyne, J. G. Georgiadis, P. M. Ferreira, J. A. Rogers, *Nat. Mater.* **2007**, *6*, 782.
- [21] B. Derby, *Annu. Rev. Mater. Sci.* **2010**, *40*, 395.
- [22] S. D. Hoath, *Fundamentals of Inkjet Printing*, Wiley-VCH, Weinheim, Germany **2016**.
- [23] J. U. Park, J. H. Lee, U. Paik, Y. Lu, J. A. Rogers, *Nano Lett.* **2008**, *8*, 4210.
- [24] R. D. Deegan, O. Bakajin, T. F. Dupont, G. Huber, S. R. Nagel, T. A. Witten, *Nature* **1997**, *389*, 827.
- [25] H. Hu, R. G. Larson, *J. Phys. Chem. B* **2006**, *110*, 7090.
- [26] J. Bohandy, B. F. Kim, F. J. Adrian, *J. Appl. Phys.* **1986**, *60*, 1538.
- [27] A. Piqué, D. B. Chrisey, R. C. Y. Auyeung, J. Fitz-Gerald, H. D. Wu, R. A. McGill, S. Lakeou, P. K. Wu, V. Nguyen, M. Duignan, *Appl. Phys. A* **1999**, *69*, S279.
- [28] P. Serra, A. Piqué, *Adv. Mater. Technol.* **2019**, *4*, 1800099.
- [29] A. Piqué, R. C. Y. Auyeung, J. L. Stepnowski, D. W. Weir, C. B. Arnold, R. A. McGill, D. B. Chrisey, *Surf. Coat. Technol.* **2003**, *163–164*, 293.

- [30] H. Kim, R. C. Y. Auyeung, S. H. Lee, A. L. Huston, A. Piqué, *Appl. Phys. A* **2009**, 96, 441.
- [31] S. M. Pozov, K. Andritsos, I. Theodorakos, E. Georgiou, A. Ioakeimidis, A. Kabla, S. Melamed, F. de la Vega, I. Zergioti, S. A. Choulis, *ACS Appl. Electron. Mater.* **2022**, 4, 2689.
- [32] G. Paris, A. Klinkusch, J. Heidepriem, A. Tsouka, J. Zhang, M. Mende, D. S. Mattes, D. Mager, H. Riegler, S. Eickelmann, F. F. Loeffler, *Appl. Surf. Sci.* **2020**, 508, 144973.
- [33] S. Eickelmann, S. Moon, Y. Liu, B. Bitterer, S. Ronneberger, D. Bierbaum, F. Breitling, F. F. Loeffler, *Langmuir* **2022**, 38, 2220.
- [34] J. Zhang, Y. Liu, S. Ronneberger, N. V. Tarakina, N. Merbouh, F. F. Loeffler, *Adv. Mater.* **2022**, 34, 2108493.
- [35] G. Paris, J. Heidepriem, A. Tsouka, Y. Liu, D. S. Mattes, S. Pinzon Martin, P. Dallabernardina, M. Mende, C. Lindner, R. Wawrzinek, C. Rademacher, P. H. Seeberger, F. Breitling, F. R. Bischoff, T. Wolf, F. F. Loeffler, *Adv. Mater.* **2022**, 34, 2200359.
- [36] Y. Liu, P. H. Seeberger, N. Merbouh, F. F. Loeffler, *Chem. - Eur. J.* **2021**, 27, 16098.
- [37] J. Zhang, Y. Zou, S. Eickelmann, C. Njel, T. Heil, S. Ronneberger, V. Strauss, P. H. Seeberger, A. Savateev, F. F. Loeffler, *Nat. Commun.* **2021**, 12, 3224.
- [38] G. G. Stokes, *Philos. Trans. R. Soc. London* **1852**, 142, 463.
- [39] B. Ridder, T. C. Foertsch, A. Welle, D. S. Mattes, C. M. von Bojnicic-Kninski, F. F. Loeffler, A. Nesterov-Mueller, M. A. R. Meier, F. Breitling, *Appl. Surf. Sci.* **2016**, 389, 942.
- [40] S. Eickelmann, A. Tsouka, J. Heidepriem, G. Paris, J. Zhang, V. Molinari, M. Mende, F. F. Loeffler, *Adv. Mater. Technol.* **2019**, 4, 1900503
- [41] F. Pedregosa, G. Varoquaux, A. Gramfort, V. Michel, B. Thirion, O. Grisel, M. Blondel, P. Prettenhofer, R. Weiss, V. Dubourg, J. Vanderplas, A. Passos, D. Cournapeau, M. Brucher, M. Perrot, E. Duchesnay, *J. Mach. Learn. Res.* **2011**, 12, 2825.